Y. Zhao, X. Qi, Y. Dong, J. Ma, Q. Zhang, L. Song, Y. Yang, Q. Yang, 2016. Mechanical, thermal and tribological properties of polyimide/nano-SiO_2 composites synthesized using an in-situ polymerization. Tribology International, 103: pp. 599-608.

Mechanical, thermal and tribological properties of polyimide/nano-SiO_2 composites synthesized using an *in-situ* polymerization

Yuanliang Zhao[1, 2], Xiaowen Qi[1, 2] *, Yu Dong[3], Jian Ma[1, 2], Qinglong Zhang[1, 2], Laizhou Song[2, 4], Yulin Yang[1, 2], Qingxiang Yang[2, 5]

[1]School of Mechanical Engineering, Yanshan University, Qinhuangdao 066004, P. R. China

[2]Aviation Key Laboratory of Science and Technology on Generic Technology of Self-Lubricating Spherical Plain Bearing,Yanshan University, Qinhuangdao 066004, P. R. China

[3]Department of Mechanical Engineering; School of Civil and Mechanical Engineering, Curtin University, Perth, WA 6845, Australia

[4]School of Environment and Chemical Engineering, Yanshan University, Qinhuangdao 066004, P. R. China

[5]School of Material Science and Engineering, Yanshan University, Qinhuangdao 066004, P. R. China

[*]Corresponding author: X. W. Qi E-Mail: qxw_tougao@163.comTel: +86 0335-8077601 Fax: +86 0335-8077601

Abstract: Polyimide (PI)/nano-SiO_2 composites were successfully fabricated via a novel *in-situ* polymerization. Microstructure, thermal properties, mechanical performance and tribological behaviors of these composites were investigated. The results indicate that nano-SiO_2 dispersed homogeneously. Compared with pure PI, thermal stability and heat resistance are higher about 10℃ with the addition of 5 wt% nano-SiO_2. Compressive strength and modulus of composite with 5 wt% nano-SiO_2 increase by 42.6 and 45.2%, respectively. The coefficient of friction (COF) of composite with 5 wt% nano-SiO_2 decrease by 6.8% owing to the thick and uniform transfer films. Excess nano-SiO_2 could adversely affect the COF of PI/nano-SiO_2 composite. Additionally, wear resistance deteriorates obviously since transfer film exfoliates easily and nano-SiO_2 aggregates on the surface of transfer films.

Keywords: *polyimide (PI)/nano-SiO_2 composites, homogeneous dispersion, mechanical and thermal properties, friction and wear*

1. Introduction

Polyimide (PI) is an excellent polymeric material due to its outstanding material performance such as high mechanical strength, acceptable wear resistance under certain conditions and good thermal stability. It is often used to fabricate PI based composites as self-lubricating bearings materials [1,2].The addition of inorganic nano-particles has been proved to be an effective way to improve thermal, mechanical and tribological properties of PI matrices. As a matter of fact, nanoparticles tend to be agglomerated into larger clusters, especially when particle contents are much higher due to the van der Waals interaction [3]. Hence, it is critical to obtain homogeneously dispersed nanoparticles in manufactured nanocomposite systems.

Typical methods employed to improve the dispersion state of nanoparticles consist of *in-situ* polymerization, melt compounding, mechanical mixing methods, etc. Minko et al. [4] synthesized PI/SiO_2 films via a sol-gel process and found that properties of PI composites were significantly improved with the addition of nano-SiO_2 particles. Liu et al. [5] investigated tribological properties of PI/nano-TiO_2 composite films via an *in-situ* polymerization. The friction coefficient and wear rate of PI/TiO_2 composites became smaller than those of pure PI at the optimum contents of 3 and 9%,

respectively in a dry sliding condition. However, the friction coefficient of PI/TiO_2 composites was shown to increase with the water lubrication. Diez-Pascual et al. [6] fabricated polyetheretherketone (PEEK)/PI composites reinforced with TiO_2 nanoparticles with the aid of ultrasonication and subsequent melt compounding. The results indicated that thermal stability, glass transition temperature and tribological properties were improved evidently with 4 wt% TiO_2. Jia et al. [7] incorporated nano-expanded graphite (EG) into PI using mechanical mixing and investigated tribological properties of PI/nano-EG composites. The addition of 15 wt% nano-EG significantly increased the wear resistance of PI matrices by 200 times. Cai et al. [8] synthesized PI/Al_2O_3 composites by incorporating nano-Al_2O_3 into PAA (precusor of PI) solution. The associated results indicated that 3 to 4 wt% nano-Al_2O_3 could improve the tribological properties remarkably. These mixing methods, especially *in-situ* polymerization, have been proven to be effective approach to improve the properties of polymer matrices. However, the dispersion state of nanoparticles is not satisfactory at higher contents and *in-situ* polymerization method is generally used in the film fabrication. But, films are not easily processed into self-lubricating bearings or self-lubricating parts, which limits the use of polymer composites. Compared with films, powders might be more suitable for self-lubricating substrate or additives.

On the other hand, among above-mentioned inorganic particles, SiO_2 nanoparticles exhibit widespread applications for the enhancements of thermal, mechanical and tribological properties. Zhang et al. [9] used a ball milling technique to disperse nano-SiO_2 particles into PEEK powders in order to evaluate tribological properties of PEEK/SiO_2 composites. Although nano-SiO_2 particles were agglomerated at high contents of 4 wt%, their incorporation led to the significant improvement for tribological properties of composites. Lai et al. [10] studied the effect of silica size on tribological performances of PI/nano-SiO_2 composites by means of the sol-gel process to disperse nano-SiO_2 particles into PI membranes. The enhancement of tribological properties is ascribed to the homogeneous dispersion of nano-SiO_2 particles at the nanoscaled level. Liu et al. [11] dispersed nano-SiO_2 particles into the PI precursor via *in-situ* polymerization and thermal imidization to fabricate PI/nano-SiO_2 composite

films. Nano-SiO_2 particles were detected to be uniformly dispersed at a low filler content of 9 wt%, but easily agglomerated at the high content level.

The above-mentioned literatures demonstrate excellent material performance for PI/nano-SiO_2 composites. Additionally, the research of PI/nano-SiO_2 molding powders is still not as much as that of PI/nano-SiO_2 films. Given these, it is very necessary to find a simple but efficient dispersion method for the application of PI/nano-SiO_2 composite powders. The objective of this study is to explore the feasibility of a novel *in-situ* polymerization on the dispersion of nano-SiO_2 particles in PI matrices and holistically investigate thermal, mechanical and tribological properties of PI/nano-SiO_2 composites.

2. Experimental details

2.1 Materials

3,3',4,4'-oxydiphthalicanhydride (ODPA) and 4,4'-oxydianiline (ODA) were supplied by Changzhou Sunchem Pharmaceutical Chemical Material Co., Ltd., China. Acetone was purchased from Tianjin Jindongtianzheng Fine Chemical Reagent Factory, China. Acetic anhydride and methylbenzene were obtained from Tianjin Kermel Chemical Reagent Co., Ltd. Triethylamine was supplied by Tianjin Guangfu Fine Chemical Research Institute, China. Nano-SiO_2 particles and 3-glycidyloxypropyltrimethoxysilane (GOTMS) were obtained from Aladdin industrial corporation, China. All other chemicals were commercially available from various sources without modification.

2.2 Preparation of PI/nano-SiO_2 composites

Acetone, nano-SiO_2 particles and GOTMS were placed into a beaker, subjected to magnetic stirring and ultrasonication for 30 min at room temperature. Subsequently, ODA was added with continuous stirring for 1 h at 50 ℃ to ensure the sufficient reaction between ODA and GOTMS. ODPA was added into the mixture in batches by stirring for 4 h to obtain PAA/nano-SiO_2 composites. Finally methylbenzene, triethylamine and acetic anhydride were stirred with the aforementioned mixture for 1 h in the imidization process. The mixture was filtrated to collect PI/nano-SiO_2 composites. Then PI/nano-SiO_2 composites were washed thoroughly with acetone and

dried at 80℃. After heat treatment at 280℃ for 2 h, PI/nano-SiO_2 composite powders were finally prepared. The material formulations of PI/nano-SiO_2 composites are listed in Table 1.

Pure PI and PI/nano-SiO_2 powders were compressed under 20 MPa at 380℃ for 1 h in a graphite mold with the cylindrical cavity (diameter: 50 mm) [1]. After released from the mold, parts with the thickness of 3 mm were cut into specimens for mechanical test and friction test, respectively.

2.3 Material characterization

The molecular structure of PI composites was characterized by Fourier transform infrared spectroscopy (FT-IR) spectra with the aid of a Nicolet IS5 FT-IR spectrometer (Thermo Fisher Co., America). In order to investigate dispersion state of nano-SiO_2 particles, the morphologies of PI/nano-SiO_2 composites (powders and molding specimen) were observed using S-4800 scanning electron microscope. The samples were sputter coated with a thin layer of gold (about 10- 20 nm) prior to the scanning electron microscopy (SEM) examination.

Thermogravimetric analysis (TGA) and differential scanning calorimetry (DSC) were performed together on a differential scanning calorimeter (STA449C, NETZSCH). Experiments were carried out on an approximately 8 mg of samples at a heating rate of 10 ℃ $min^{-1}$from 35 to 1000 ℃ in air and argon atmosphere.

Mechanical properties were obtained using both compression and hardness tests. Compression tests were conducted by using a universal testing machine (WDW3100 KeXin, China) according to GB/T 1041-2008 (ISO 604-2002). Specimen was cut into size: 5 mm×6 mm×3 mm and compressive strength was recorded at strain 10%. Furthermore, the Shore hardness of PI/nano-SiO_2 composites was measured using a digital durometer *D* (Shore) according to GB/T 2411-2008 (ISO 868:2003). The reported average data were based on at least three samples for each test for good reproducibility.

2.4 Friction and wear tests

Friction and wear behavior of PI/nano-SiO_2 composites were evaluated on a reciprocating ball-on-disc friction and wear tester (i.e. CSM Tribometer). To match

the tribometer, the size of friction test specimen is 18 mm×10 mm×3 mm. For friction and wear tests, sliding was performed under ambient environment for 1.5 h at sliding velocities of 0.08 and 0.04 m/s under the normal loads of 5 and 10 N. The ambient environment was at room temperature and humidity. Prior to each test, sample surfaces were polished using water-abrasive papers. Further, the specimen and GCr15 ball with 3 mm in diameter were cleaned with acetone using ultrasonication for 20 min prior to drying. The dimensions of wear scar on the surface of specimens were measured with a three dimensional surface measuring instrument at the end of each test. The wear volume loss, *V*, of the block specimen was calculated based on the following equation [12]:

$$V = B\left[\frac{\pi}{180}R^2 \arcsin\frac{b}{2R} - \frac{b}{2}\sqrt{R^2 - \frac{b^2}{4}}\right] \quad (1)$$

where *V* is the wear volume loss (mm^3), *B* is the wear track length of the sample (mm), *b* is the wear track width (mm), and *R* is the radius of GCr15 ball (mm). The wear resistance of PI/nano-SiO_2 composites was determined by the formula [12]:

$$K = \frac{V}{FL} \quad (2)$$

where *K* is specific wear rate ($mm^3(N\cdot m)^{-1}$) of PI/nano-SiO_2 composites, *F* is the load (N) an *L* is the sliding distance (m). To minimize experimental errors, the final data were obtained by averaging the results from three repeated tests. Finally, wear surfaces and transfer films were inspected by SEM micrographs.

3. Results and discussion

3.1 FT-IR analysis

FT-IR spectra of nano-SiO_2 and PI/nano-SiO_2 composites with different nano-SiO_2 contents were revealed in Fig. 1(a). The spectrum of nano-SiO_2 exhibits a wide peak at 3434 cm^{-1}, which is attributed to the O-H stretching [13]. The intense absorption peak at 1089 and 469 cm^{-1} arises from the Si-O-Si stretching and bending vibration [14], respectively. The peaks of imide rings are at 1711 cm^{-1} for C=O symmetric stretching and 1777 cm^{-1} for C=O asymmetric stretching in the spectrum of pure PI [15]. The characteristic peaks of imide rings can also be found in PI/nano-SiO_2

composites. Nonetheless, the characteristic band of the amide carbonyl at 1650 cm^{-1} is invisible, signifying the complete imidization reaction taking place. In addition, it can be observed that the peak intensities of Si-O-Si stretching with a sign of being overlapped with the peaks of PI in the 1000 - 1100 cm^{-1} region and bending vibration are enhanced gradually with increasing the nano-SiO_2 contents.

FT-IR spectra of pure PI and PI/nano-SiO_2 composites with the nano-SiO_2 content of 20 wt% before and after 280℃ treatment are shown in Fig. 1(b). The absorption peak at 1545 cm^{-1} (i.e. N-H deviational vibration and C-N stretching) implies that the chemical imidization is insufficient, and this peak disappeared after 280℃ heat treatment. Compared with pure PI, PI/nano-SiO_2 composites before 280℃ treatment displayed a typical peak for -CH_2- absorption at 2938 cm^{-1}, which indicates that the coupling agent GOTMS plays an effective role in achieving better interactions between PI and nano-SiO_2 particles. As evidenced by the higher wave number of composites for imide peaks assigned to C=O vibration than that of pure PI, a spectral blue shift [16] is demonstrated owing to the strong interactions between the coupling agent and other components. After 280℃ treatment, the major portion of -CH_2- absorption peak has disappeared and the wave number of composite imide peaks for C=O vibration is still higher than that of pure PI. These phenomena illustrate there is still weak interactions between the coupling agent and other components.

3.2 Morphology analysis

In general, mechanical and tribological properties of polymer based nanocomposites are influenced by the dispersion state of nanofillers [11]. Given this, to better investigate the distribution of nano-SiO_2 particles in PI matrices, morphological structures of PI/nano-SiO_2 powders and fracture surface of their molding specimens were observed at the nano-SiO_2 content of 20 wt%. SEM and backscattered (BSE) morphologies of PI/nano-SiO_2 powders are shown in Fig. 2(a, b). The surface of PI/nano-SiO_2 particles exhibits little sign of SiO_2 re-aggregation, which reveals the uniform dispersion of nano-SiO_2 particles on the surface of PI powders. To further study the dispersion state of nano-SiO_2, the surface of hot-pressed specimen was used to conduct the silicon mapping in Fig. 2(c, d). As can be seen, Si

atoms (light dots) are dispersed homogeneously in PI matrices and the distribution of Si atoms is similar to that shown in the previous literature [15], which further confirms that nano-SiO_2 particles are homogeneously dispersed within PI matrices. Moreover, the fracture surface of hot-pressed specimen was observed using field emission scanning electron microscope (FESEM), and the high-magnification micrograph of the surface is depicted in Fig. 2(e). It can be observed that the fracture surface is relatively smooth without a clear evidence of agglomerated nano-SiO_2 particles [11], implying the uniform dispersion of nano-SiO_2 particles. Hence, it can be concluded that nano-SiO_2 particles are dispersed homogeneously into PI matrices with this polymerization method, even at higher nano-SiO_2 content of 20 wt%. The homogenous dispersion of nano-SiO_2 particles may be associated with the better interaction between monomers and nanoparticles with the existence of coupling agents [17], as well as PAA to facilitate the segregation of nanoparticles for the fabrication of such composites [18].

3.3 Thermal properties

TG curves and DSC traces are shown in Fig. 3 to investigate the thermal stability and heat resistance of PI/nano-SiO_2 composites, respectively. And the results are summarized in Table 2.

As shown in Fig. 3(a), weight loss (2.5 - 4%) of PI/nano-SiO_2 composites is higher than that of pure PI at 2.5% between 300 and 500℃. This phenomenon might be attributed to the use of silane coupling agent (GOTMS), since the decomposition temperature of aliphatic group is lower than that of PI matrices [19]. From Table 2, T_5 and T_{10} of PI/nano-SiO_2 composites are in the range of 516.3 ~ 544.0 ℃ and 554.6 ~ 565.8 ℃ respectively, which illustrates PI/nano-SiO_2 composites have excellent thermal stability. T_{10} values of PI/nano-SiO_2 composites are higher than or equal to that of pure PI (554.6 ℃). T_5 values of PI/nano-SiO_2 with 5 and 25 wt% nano-SiO_2 are higher up to 11.5 and 10℃than that of pure PI (532.5 ℃) obviously, but *those* of PI/nano-SiO_2 are lower than that of pure PI when nano-SiO_2 content is in the range of 10 to 20 wt%. This phenomenon means that nano-SiO_2 contribute to the degradation

of PI matrices when its content is above 10 wt%, since excess high SiO_2 content causes negative effects on composites' thermal properties [20]. Similar phenomenon was observed in PI/nano-SiO_2 films when SiO_2 content is higher (13 wt%) [11] and (67.42 wt%) [20]. They attributed this phenomenon to the following reasons: first, the motion and reaction of PI molecules were hindered with the increase of nano-SiO_2 particles, which enhance the thermal stability of PI matrix; second, crosslink structure of PI matrices was broken and the phase separation size increased at high nano-SiO_2 content, which deteriorated the thermal stability of PI matrix. The second effect plays an important role in the degradation of PI matrices when nano-SiO_2 content is higher. Compared with literature [11, 20], the second effect was enhanced at lower nano-SiO_2 content (10 wt%) using our dispersion method, which might be because nano-SiO_2 is more homogeneously in our study. Meanwhile, the first effect was enhanced with the increase of nano-SiO_2 content [19], which caused upward trend in decomposition temperature with the increase of nano-SiO_2 content (10 – 25 wt%). As illustrated in Fig. 3(a), above 600 ℃, the maximum decomposition rate of composites with various nano-SiO_2 contents ranged in the following order: 0 wt% > 25 wt% > 20 wt% > 15 wt% > 10 wt% > 5 wt%. The decomposition rate of PI/nano-SiO_2 composites, which is lower than that of pure PI, increases with the increase of nano-SiO_2 content. This means that thermal stability of PI/nano-SiO_2 composites is higher than that of pure PI and decreases with the increase of nano-SiO_2 content when temperature is above 600℃. Appropriate amounts of nanoparticles restrict the thermal decomposition of PI matrices, which is ascribed to the use of nano-SiO_2 particles to delay the escape of decomposition products from PI/nano-SiO_2 composites at high temperature [21]. However, nano-SiO_2 dispersed homogeneously in PI matrix and thermal conductivity of nanocomposites is relative higher than that of polymer matrix [22, 23], which means that the thermal conductivity of PI/nano-SiO_2 increases with the increase of nano-SiO_2 content. Therefore, PI matrix might be heated evenly and oxidized easily, which will increase the oxide decomposition rate of PI matrix at high temperature (above 600 ℃).

TG curves can also be used to demonstrate the real composition of nano-SiO_2

particles in PI matrices [24,25]. Meanwhile, the mainly composition of PI/nano-SiO_2 composites includes PI, nano-SiO_2 and GOTMS, so the residuals of oxidation decomposition were SiO_2. The residuals of PI/nano-SiO_2 composites were corresponding to the expected content of nano-SiO_2 as shown in Table 2, which indicates that the addition of expected nano-SiO_2 proportion into PI matrix was successful.

On the other hand, the heat resistance of PI/nano-SiO_2 composites can be evaluated from Fig. 3(b) and Table 2. The glass transition temperatures (T_g) of composites are in range of 256.6 ~ 265.2 ℃, which is higher up to 6.6 ~ 15.2 ℃ than that of pure PI (T_g = 250 ℃). This finding can result from the hindrance of PI chain movements owing to dispersed nano-SiO_2 particles [26]. Although T_g of PI/nano-SiO_2 composites slightly fluctuates with increasing the nano-SiO_2 content, the heat resistance of PI/nano-SiO_2 composites is much better than that of pure PI.

3.4 Mechanical properties

Shore hardness, compressive strength and compressive modulus are essential mechanical properties for the application of PI/nano-SiO_2 composites, whose results are shown in Fig. 4. Shore hardness of PI/nano-SiO_2 composites is higher than that of pure PI, which also increases significantly with the increase of nano-SiO_2 content, as shown in Figure 4(a). This phenomenon could be explained by the high hardness of nano-SiO_2 particles and strong interfacial interaction between PI and nano-SiO_2 particles [27].

Compared with the strength of pure PI (88.02 MPa), PI/nano-SiO_2 composites possess higher values (125.51 ~ 128.73 MPa) with the increasing level over 42.6% when nano-SiO_2 content is 5 ~20 wt%, as shown in Figure 4(b). After an initial enhancement when increasing the nano-SiO_2 contents from 0 to 5 wt%, the compressive strength tended to reach the retention with the increase of nano-SiO_2 content from 5 to 20 wt%, the compressive strength finally decreased when increasing nano-SiO_2 content from 20 to 25 wt%. This phenomenon was attributed to the counterbalance of following reasons: first, addition of nano-fillers make composites

more compact and nano-fillers could absorb a portion of crack energy [28], thus resulting in the improvement of mechanical properties of composites. Second, the content of polymer substrate reduces with the increase of fillers and induces stress concentration sites in polymer matrices [9], which caused the decrease in mechanical performance. In addition, the aggregation of nano-fillers is inevitably with the increase of fillers content, which leads to the deterioration of mechanical performance. Therefore, mechanical performance of nanocomposites increases at first and then decreases with the increase of nano-fillers content. This phenomenon is similar to the mechanical performance of PI modified by clay [29], Al_2O_3 [8] and SiO_2 [19]. However, compressive strength reached retention with the increase of nano-SiO_2 content from 5 to 20 wt% in our study. The difference might be mainly attributed to the more evenly dispersed state of nano-SiO_2 and stronger adhesion strength of GOTMS than literature.

More interestingly, compressive modulus exhibits a similar trend with compressive strength, as shown in Fig. 4(b). The optimum compressive modulus of PI/nano-SiO_2 composites (1.75~1.77 GPa) are 45.2% higher than that of pure PI (1.21 GPa). These improvements can be due to the strong reinforcement of homogeneously dispersed nano-SiO_2 particles and good interfacial adhesion between PI and nano-SiO_2 particles accordingly [30]. All of above illustrate that PI/nano-SiO_2 composites possess much better mechanical properties than that of pure PI, which also coincide with the fact that nano-SiO_2 can act as effective fillers for the application of additive reinforcements [10, 11].

3.5 Friction and wear properties

Coefficient of friction (COF) curves of PI/nano-SiO_2 composites with different nano-SiO_2 contents as a function of time at the load of 10 N and sliding velocity of 0.08 m/s and their average values are shown in Fig. 5. From Fig. 5(b), it can be concluded that the addition of nano-SiO_2 is beneficial to the reduction of COF when nano-SiO_2 content is below 10 wt%, especially with the lowest level of 0.274 at 5 wt% as opposed to 0.294 for that of pure PI. Such a finding may lie in homogeneous dispersion of nano-SiO_2 particles and strong interfacial interaction between PI

matrices and nano-SiO_2 [30]. Meanwhile, wear debris act as rollers in contact zone, which change sliding friction to rolling friction [31]. Therefore, COF of PI/nano-SiO_2 composites decreases when the content of nano-SiO_2 particles is lower. However, with the increase of amounts of nanoparticles, nanoparticles promote the spalling of polymer matrices and produce more debris, which cause severe abrasive wear [28]. Therefore, the COF of PI/nano-SiO_2 composites increases when the content of nano-SiO_2 particles is in the range of 5 ~25 wt%. As shown in Fig. 5(b), wear rate of PI composites is higher than that of pure PI and is about 2 orders magnitude higher than literatures [32, 33, 34]. It should be noted that the PI/nano-SiO_2 composites in current study is structurally different from those in literatures, which is directly resulted from the *in-situ* synthesis strategy that applied here. In this paper, nano-SiO_2 particles were dispersed into 3,3',4,4'-oxydiphthalicanhydride (ODA) to directly participate in the synthesis of PI/nano-SiO_2 composites (as described in *Experimental details*), which is essentially different from the mechanical blending of PI products and additives used in references [32-34]. One of the direct outcomes of the *in-situ* synthesis strategy is the varied molecular weight of PI/SiO_2 composites [35], which is highly associated with the tribological properties of the PI-based composites [1, 36] and the crosslinking reaction in molding process—another aspect that affects the tribological properties of PI-based composites [11, 37]. In addition, the deteriorated bonding strength between the transfer film and the counterpart surface might be another aspect that responsible for the decreased wear resistance of the PI/nano-SiO_2 composites [38]. This is apparently demonstrated by the local exfoliation of the transfer films (as shown in Fig. 8 at section 3.6), resulting in the dramatic increase in the wear rate of the PI/nano-SiO_2 composites [38].

In addition, the COF and wear rate of PI/nano-SiO_2 composites at different loads were studied at a sliding velocity of 0.08 m/s with the relevant results shown in Fig. 6. It can be seen that the COF have a similar trend as a function of nano-SiO_2 content at light and heavy loads, as shown in Fig. 6(a). In addition, the COF for 5 wt % nano-SiO_2 particles is the lowest at both light and heavy loads of 5 and 10 N. Besides, the main trend is that a relatively small COF was displayed at heavy load, which

indicates that composites are slightly suitable for the overloading condition. This can be theoretically explained by the equation $\mu = kN^{n-1}$ (where μ is the COF, N is the load, k and n are constants where n is in the range from 2/3 to 1) [39]. As shown in Fig. 6(b), the wear rate of PI/nano-SiO_2 composites is much higher than that of pure PI. The wear rate initially increases significantly when increasing the nano-SiO_2 contents from 0 to 5 wt%, and then becomes nearly level-off in the range of 5-20 wt%. Further moderate enhancement of wear rate is evident when the nano-SiO_2 content reaches 25 wt%. As abrasive wear generally acts as the major wear characteristic for composites with high filler content levels, the intensification of abrasive wear occurs with the load increase [40]. Meanwhile, the wear rate under light load is relatively small as opposed to that under heavy load, revealing that composites with higher nano-SiO_2 contents tend to be more wear resistant under light load.

Fig. 7 shows the effects of nano-SiO_2 content on the COF and wear rate of PI/nano-SiO_2 composites under two different sliding velocities of 0.04 and 0.08 m/s with the load at 10 N. From Fig. 7(a), the COF of PI/nano-SiO_2 composites at 0.04 m/s is higher than that at 0.08 m/s when nano-SiO_2 content is below 5 wt %. However, above the nano-SiO_2 content of 10 wt% (except 20 wt%), COF of PI/nano-SiO_2 composites at 0.04 m/s appears to be lower than that at 0.08 m/s. Notwithstanding that viscous resistance is improved with the increase of sliding velocity, elastic behavior of materials is the main component to diminish the effect of viscous resistance, and contact time is short in the contact zone at the high sliding velocity [41]. The high nano-SiO_2 content induces more debris in the contact zone at the high velocity, in turn resulting in the increase of COF, which coincides with the main trend of wear rate at different sliding velocities.

3.6 SEM analysis of worn surfaces and transfer films

The morphologies of worn surfaces and transfer films of PI/nano-SiO_2 composites sliding against GCr15 steel ball at 0.08 m/s and 10 N are shown in Fig. 8. The friction force can be decomposed into interfacial adhesion and plowing [42], leading to both adhesive and abrasive wears on the sliding surfaces of PI/nano-SiO_2 composites. On

the other hand, the frictional force is generally influenced by mechanical properties and friction heat of specimens [43]. The addition of nano-SiO_2 particles impacts mechanical and thermal properties of PI/nano-SiO_2 composites, as evidenced in Figs. 3 and 4, respectively. Consequently, the wear mechanism is altered with the increase of nano-SiO_2 contents.

As shown in Fig. 8(a_1), the worn surface of PI/nano-SiO_2 composites with the nano-SiO_2 content of 5 wt% is smooth and characterized by slight scuffing resulting from abrasive wear. Additionally, there exists tiny debris on the worn surfaces. Transfer films of PI/nano-SiO_2 composites with the nano-SiO_2 content of 5 wt% is thick and uniform relatively (Fig. 8a_2), which suggests that adhesive and abrasive wear play an important role in wear mechanism [44].Owing to the dominant adhesion wear, the worn surfaces of pure PI is rough and severe scuffing; the transfer film is thick, lumpy and unevenness [8, 3939]. Addition of nano-SiO_2 causes tremendous changes on worn surfaces and transfer films, which are consistent with the lowest COF of PI/nano-SiO_2 composites with the nano-SiO_2 content of 5 wt%. However, the toughness of PI composites decreases with the addition of nano-SiO_2 particles [9], which promoted the spalling of the PI matrices and generated more debris between friction pairs [28]. Meanwhile, exfoliation of the transfer films (Fig. 8a_2) indicates that bonding strength between transfer films and counterpart is lower under the experiment conditions of this paper [38]. Therefore, direct contact between specimens and counterpart increase the wear rate of PI composites. In other words, wear resistance of PI/nano-SiO_2 composites with 5 wt% nano-SiO_2 is lower (Fig. 5b). When nano-SiO_2 content reaches 10 wt%, obvious bulges can be detected on worn surfaces without scratches (Fig. 8b_1). This phenomenon means that the dominant wear mechanism was transformative from adhesive wear to abrasive wear as nano-SiO_2 content increasing. The thicker and wider transfer film contributes to the decrease of wear rate when nano-SiO_2 content increases from 5 to 10 wt%, although local transfer films peels off obviously (Fig. 5). When nano-SiO_2 content increases up to 15 wt%, the deterioration of worn surface morphology is observed, along with some deep furrows and micro-pits on worn surfaces (Fig. 8c_1). The occurrence of scratches

implies serious abrasive characteristic existing in the wear system to deteriorate the friction. This finding is also confirmed with many wear debris and nano-SiO_2 aggregates on the surface of transfer film, as illustrated in Fig. $8c_2$. As a result, the aggregation of nano-SiO_2 particles on the surface of transfer film can scratch the surface of specimens, which increases the wear rate of PI/nano-SiO_2 composites. Typical scratches, micro-pits and micro-cracks are observed on the worn surface morphology when nano-SiO_2 content increases up to 20 wt% (Fig. $8d_1$). This phenomenon presents that abrasive wear and fatigue wear act as major wear forms. Compared with nano-SiO_2 content of 15 wt% (Fig. $8c_2$), slight agglomeration of nano-SiO_2 particles is visible on the surface of wide and thin transfer films (Fig. $8d_2$), which induces the slight increase of wear resistance of PI/nano-SiO_2 composites (Fig. 5b). In conclusion, the dominant wear mechanism of PI/nano-SiO_2 composites is abrasive wear, which induces the decrease of COF because wear debris act as rollers at lower SiO_2 content [31]. Meanwhile, wide, smooth and uniform transfer film is beneficial to the improvement of tribological properties of PI/nano-SiO_2 composites. However, bonding strength between transfer films and counterpart is lower under the experiment conditions of this paper, which lead to the local exfoliation of the transfer films at lower SiO_2 content (Fig. $8a_2$, b_2) and rough edges of transfer films at higher content (Fig. $8c_2$, d_2). Therefore, direct contact between composites and counterpart is one of the aspects for the poor wear resistance of PI/nano-SiO_2 composites [38]. In addition, aggregation of nano-SiO_2 on the surface of transfer films at higher SiO_2 content increases the hardness of transfer films and scratches the surface of PI composites as shown in Fig. $8c_2$, d_2, which is also responsible for the high wear rate of PI/nano-SiO_2 composites.

Furthermore, EDS results of transfer films were further analyzed on the abrasion mechanism with corresponding results shown in Fig. 9. Meanwhile, smart quant results of transfer films were summarized in Table 3. The main components of transfer films contain C, O, Si, Fe and Cr. The existence of C, O and Si implies that the debris of PI/nano-SiO_2 composites adheres to the surface of steel ball. Considering the small thickness of transfer films, their components suggest that Fe and Cr peaks stems

mainly from GCr15 counterpart ball. With the increase of nano-SiO_2 content, the mass of elements in transfer films changes significantly, which suggests that the thickness of transfer films varies with the increase of nano-SiO_2 contents. The thickness of transfer films for different nano-SiO_2 contents may be in the following sequence: 10 wt% > 5 wt% > 15 wt% >20 wt%, which is in good accordance with the results obtained in Figs. 8(a_2, b_2, c_2, d_2).

Conclusions

In this study, PI/nano-SiO_2 composite powders were synthesized successfully using this novel polymerization. And the effects of nano-SiO_2 particles on thermal, mechanical and tribological properties of PI/nano-SiO_2 composites have been successfully evaluated. High thermal resistance, excellent mechanical and antifriction properties and poor wear resistance may make it a potential material for the application of self-lubricating bearings with the requirement of low friction coefficient in discontinuous operation. The associated results are summarized as follows:

- Homogeneously dispersed nano-SiO_2 particles at high content levels were achieved within PI/nano-SiO_2 composite powders when this *in-situ* polymerization process was successfully employed.
- In comparison with pure PI, much better thermal stability and thermal resistance were obtained for PI/nano-SiO_2 composites with nano-SiO_2 content at 5 wt%. Meanwhile, thermal stability tended to become worse with the nano-SiO_2 content at 10 wt% and then improved with the increase of nano-SiO_2 content from 10 to 25 wt%.
- With nano-SiO_2 contents of 5 - 20 wt%, the compressive strength of PI/nano-SiO_2 composites was increased about 42.6% and compressive modulus is 45.2% higher than that of pure PI. Meanwhile, the increment of hardness was shown to be associated with the nano-SiO_2 contents between 0 - 25 wt% in a linear relationship. The COF of PI/nano-SiO_2 composites was initially decreased by 6.8% with increasing the nano-SiO_2 contents from 0 wt% to 5 wt%, and then was increased by 11% with increasing the nano-SiO_2 contents from 5 to 25 wt%. The lowest COF

was observed at nano-SiO_2 contents in the range of 5-10 wt% while the wear rate of PI/nano-SiO_2 composites at present nano-SiO_2 content became higher than that of pure PI. Nano-SiO_2 in the range of 5-10 wt% could be used to effectively restrict the adhesive wear and promote the decreasing of COF. Since transfer film exfoliates easily and nano-SiO_2 tends to amass on the surface of transfer films, wear resistance of PI/nano-SiO_2 composites is deteriorated.

References

[1] Wang YM, Wang TM, Wang QH. Effect of molecular weight on tribological properties of thermosetting polyimide under high temperature. Tribol Int, 2014; 78(4):47–59.

[2] Roberts E W. Space tribology: its role in spacecraft mechanisms. J Phys D: Appl Phys 2012; 45(50):503001-503017.

[3] Giannelis, Emmanuel P. Polymer layered silicate nanocomposites, Adv Mater 1996; 8(1): 1-9.

[4] Minko E, Bershtein V, Sysel P, Egorova L. Hyperbranched polyimide-silica hybrid materials: synthesis, structure, dynamics and gas transport properties. J Macromol Sci Phys 2013; 52(4): 632-649.

[5] Liu H, Wang TM, Wang QH. Tribological properties of thermosetting polyimide/TiO_2 nanocomposites under dry sliding and water-lubricated conditions. J Macromol Sci Phys 2012; 51 (11): 2284–2296.

[6] Diez-Pascual AM, Diez-Vicente AL. Nano-TiO_2 reinforced PEEK/PEI blends as biomaterials for load-bearing implant applications. ACS Appl Mater Inter 2015; 7(9): 5561-5573.

[7] Jia ZN, Hao CZ, Yan YH, Yang YL. Effects of nanoscale expanded graphite on the wear and friction behaviors of polyimide-based composites. Wear 2015; 338: 282-287.

[8] Cai H, Yan FY, Xue QJ, Liu WM. Investigation of tribological properties of Al_2O_3-polyimide nanocomposites. Polym Test 2003; 22(8): 875–882.

[9] Zhang G, Schlarb AK,Tria S,. Elkedim O. Tensile and tribological behaviors of PEEK/nano-SiO_2 composites compounded using a ball milling technique. Compos Sci Technol 2008; 68(15-16): 3073-3080.

[10] Lai SQ, Li TS, Wang FD, Li XJ, Yue L, The effect of silica size on the friction

and wear behaviors of polyimide/silica hybrids by sol-gel processing, Wear 2007; 262(9): 1048-1055.

[11] Liu H, Wang TM, Wang QH. In situ synthesis and properties of PMR PI/SiO_2 nanocomposites. J Appl Polym Sci 2012; 125(1); 488-493.

[12] Peng QY, Cong PH, Liu XJ, Liu TX, Huang S, Li TS. The preparation of PVDF/clay nanocomposites and the investigation of their tribological properties. Wear 2009; 266(7-8): 713-720.

[13] Lu S, Chung TS. In situ fabrication of cross-linked PEO/silica reverse-selective membranes for hydrogen purification. Int J Hydrogen Energy 2009; 34(15): 6492-6504.

[14] Kwon Y, Im H, Kim J. Effect of PMMA-graft-silica nanoparticles on the gas permeation properties of hexafluoroisopropylidene-based polyimide membranes. Sep PurifTechnol 2011; 78(3): 281-289.

[15] Kizilkaya C, Sevim K, Apohan NK, Giingor A. Synthesis and characterization of novel polyimide/SiO_2 nanocomposite materials containing phenylphosphine oxide via sol-gel technique. J Appl Polym Sci 2010; 115(6): 3256-3264.

[16] Gao LX, Liu QP, Gao ZW, Lin Y. Preparation and characterization of Polyimide/silica-barium titanate nanocomposites. Polym Compos 2007; 29(10): 1160-1164.

[17] Shi XZ, Duan JP, Lu JJ, Liu MQ, Shi LJ. A novel fabrication method of network-like polyimide/silica composite microspheres with a high SiO_2 content. Mater Lett 2014; 128: 5-8.

[18] Zhang GL, Ke YC, He J, Qin M, Shen H, Lu SC, Xu JS. Effects of organo-modified montmorillonite on the tribology performance of bismaleimide based nanocomposites. Mater Des 2015; 86: 138-145.

[19] Al-Kandary S, Ali A A M, Ahmad Z. New polyimide-silica nano-composites from the sol-gel process using organically-modified silica network structure. J Mater Sci 2006; 41(10):2907-2914.

[20] Zhong SH, Li CF, Xiao XF. Preparation and characterization of polyimide–silica hybrid membranes on kieselguhr–mullite supports. J Membrane Sci 2002; 199(1):53-58.

[21] Patel HA, Somani RS, Bajaj HC, Jasra RV. Preparation and characterization of phosphonium montmorillonite with enhanced thermal stability. Appl Clay Sci 2007;

35(3-4): 194–200.

[22] Dai W, Yu J, Liu Z. Enhanced thermal conductivity and retained electrical insulation for polyimide composites with SiC nanowires grown on graphene hybrid fillers. Composites Part A 2015; 76:73-81.

[23] Wong C P, Bollampally R S. Thermal conductivity, elastic modulus, and coefficient of thermal expansion of polymer composites filled with ceramic particles for electronic packaging. J Appl Polym Sci 1999; 74(14):3396-3403.

[24] Lin JJ, Wang XD. Novel low-*k* polyimide/mesoporous silica composite films: preparation, microstructure, and properties. Polymer 2007; 48: 318-329.

[25] Cheng CF, Cheng HH, Cheng PW, Yuehju Lee YH. Effect of reactive channel functional groups and nanoporosity of nanoscale mesoporous silica on properties of polyimide composite. Macromolecules 2006; 39(22): 7583-7590.

[26] Lee T, Park SS, Jung Y, Han S, Han D. Preparation and characterization of polyimide/mesoporous silica hybrid nanocomposites based on water-solube poly(amic acid) ammonium salt. Eur Polym J 2009; 45(1): 19-29.

[27] Kizilkaya C, Sevim K, Apohan NK, Giingor A. Synthesis and characterization of novel polyimide/SiO_2 nanocomposite materials containing phenylphosphine oxide via sol-gel technique. J Appl Polym Sci 2010; 115(6): 3256-3264.

[28] Jiang W, Jin X, Zhang H. Poly(ether ether ketone)/wrapped graphite nanosheets with poly(ether sulfone) composites: Preparation, mechanical properties, and tribological behavior. J Appl Polym Sci 2014; 132(14).

[29] Agag T, Koga T, Takeichi T. Studies on thermal and mechanical properties of polyimide–clay nanocomposites. Polymer, 2001; 42(8):3399-3408.

[30] Wan YJ, Tang LC, Gong LX, Yan D, Li YB, Wu LB. Grafting of epoxy chains onto grapheme oxide for epoxy composites with improved mechanical and thermal properties. Carbon 2014; 69(2): 467-480.

[31] Shi Y, Mu L, Feng X. The tribological behavior of nanometer and micrometer TiO_2 particle filled polytetrafluoroethylene/polyimide. Mater Des 2011; 32(2):964-970.

[32] Tewari, Bijwe. Comparative studies on sliding wear of polyimide composites. Compos 1991 22 (3); 204-210.

[33] K. Friedrich. Sliding wear performance of different polyimide formulations, Tribol Int, 1989; 22 (1): 25-31.

[34] J.P. Giltrow. Friction and wear of some polyimides. Tribol 1973; 6(6): 253-257.
[35] Min CK, Wu TB, Yang WT. Functionalized mesoporous silica/polyimide nanocomposite thin films with improved mechanical properties and low dielectric constant. Compos Sci and Technol 2008; 68(6): 1570-1578.
[36] Moghbelli E, Browning RL, Boo WJ. Effects of molecular weight and thermal history on scratch behavior of polypropylene thin sheets. TribolInt 2008; 41(41):425-433.
[37] Jeng MC, Fung CP, Li TC. The study on the tribological properties of fiber-reinforced PBT composites for various injection molding process parameters. Wear, 2002; 252(11):934-945.
[38] Bahadur S, Sunkara C. Effect of transfer film structure, composition and bonding on the tribological behavior of polyphenylene sulfide filled with nano particles of TiO_2, ZnO, CuO and SiC. Wear 2005; 258(9):1411-1421.
[39] Zhang XR, Pei XQ, Wang QH. Friction and wear studies of polyimide composites filled with short carbon fibers and graphite and micro SiO_2. Mater Des 2009; 30(10): 4414-4420.
[40] Friedrich K, Flock J, Varadi K, Neder Z. Experimental and numerical evaluation of the mechanical properties of compacted wear debris layers formed between composite and steel surfaces in sliding contact. Wear 2001; 251(1-12): 1202-1212.
[41] Myshkin NK, Petrokovets MI, Kovalev AV. Tribology of polymers: adhesion, friction, wear, and mass-transfer. Tribol Int 2006; 38:910-921.
[42] Sun JP, Fang L, Han J, Han Y, Chen HW, Sun K. Abrasive wear of nanoscale single crystal silicon. Wear 2013; 307(1-2): 119-126.
[43] Lva M, Zheng F, Wang QH, Wang TM, Liang YM. Effect of proton irradiation on the friction and wear properties of polyimide. Wear 2014; 316(1-2): 30-36.
[44] Menezes PL, Kishore, Kailas SV, Lovell MR. Friction and transfer layer formation in polymer-steel tribo-system: role of surface texture and roughness parameters. Wear 2011; 271(9): 2213-2221.

Tables

Table 1 The composition of PI/nano-SiO_2 composites

Sample	ODA (g)	ODPA (g)	Nano-SiO_2 (g)	GOTMS (g)	SiO_2 (wt%)
PI	6.0	9.23	0	0	0
PI/SiO_2 (5wt%)	6.0	9.23	0.72	0.07	4.5
PI/SiO_2 (10wt%)	6.0	9.23	1.52	0.15	9.1
PI/SiO_2 (15wt%)	6.0	9.23	2.41	0.24	13.6
PI/SiO_2 (20wt%)	6.0	9.23	3.41	0.34	18.1
PI/SiO_2 (25wt%)	6.0	9.23	4.55	0.45	22.7

Note that weight fractions of nano-SiO_2 particles in PI/nano-SiO_2 composites were calculated from the initial amounts of nano-SiO_2 and GOTMS within PAA, assuming that ODA and ODPA react completely. Meanwhile, content of nano-SiO_2 was determined from literature [11].

Table 2 Thermal decomposition temperatures of PI and PI/nano-SiO_2 composites

Sample	T_g (℃)	T_5 (℃)	T_{10} (℃)	T_c (℃)	Residual (wt %)
PI (0wt%)	250	532.5	554.6	698.0	0.04
PI/SiO_2 (5wt%)	261.4	544.0	565.8	933.4	5.17
PI/SiO_2 (10wt%)	258.4	516.3	554.6	881.7	9.06
PI/SiO_2 (15wt%)	260.3	525.5	554.6	844.8	14.01
PI/SiO_2 (20wt%)	256.6	528.5	557.2	780.2	19.28
PI/SiO_2 (25wt%)	265.2	542.2	563.5	734.3	26.42

T_g: temperature for glass transition; T_5: temperature for 5% weight loss; T_{10}: temperature for 10% weight loss; T_c: temperature for complete decomposition; Residual: weight at 950 ℃.

* There is no apparent T_g transformation for pure PI in DSC, its literature value from reference [1] was used in Table 2 instead.

Table 3 EDS smart quant result summary for transfer films

Sample	Transfer film element			
	C (wt %)	Cr (wt %)	Fe (wt %)	Si (wt %)
PI/SiO_2 (5%)	68.7	3.79	13.75	2.51
PI/SiO_2 (10%)	72.3	1.82	6.10	2.14
PI/SiO_2 (15%)	58.9	4.10	15.52	7.02
PI/SiO_2 (20%)	51.2	5.26	20.81	5.73

Figure Captions

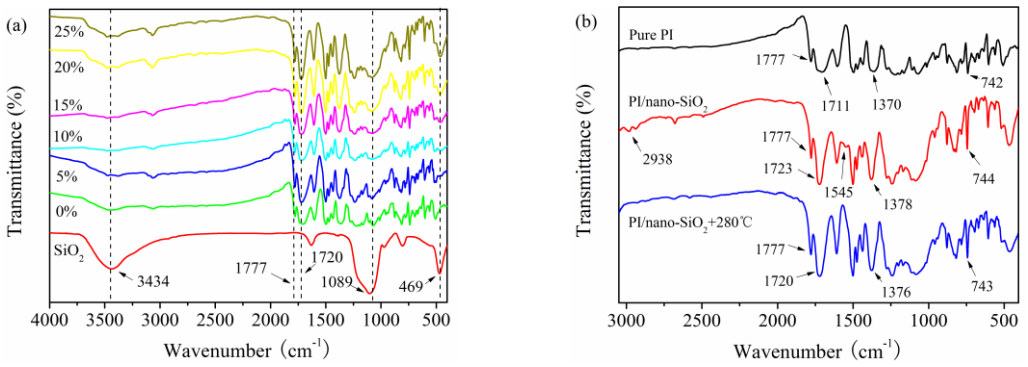

Fig. 1 FT-IR spectra of (a) nano-SiO_2 particles and PI/nano-SiO_2 composites with different nano-SiO_2 contents after 280 ℃ treatment; (b) pure PI, PI/nano-SiO_2 composites with the nano-SiO_2 content of 20 wt% before and after 280℃ treatment.

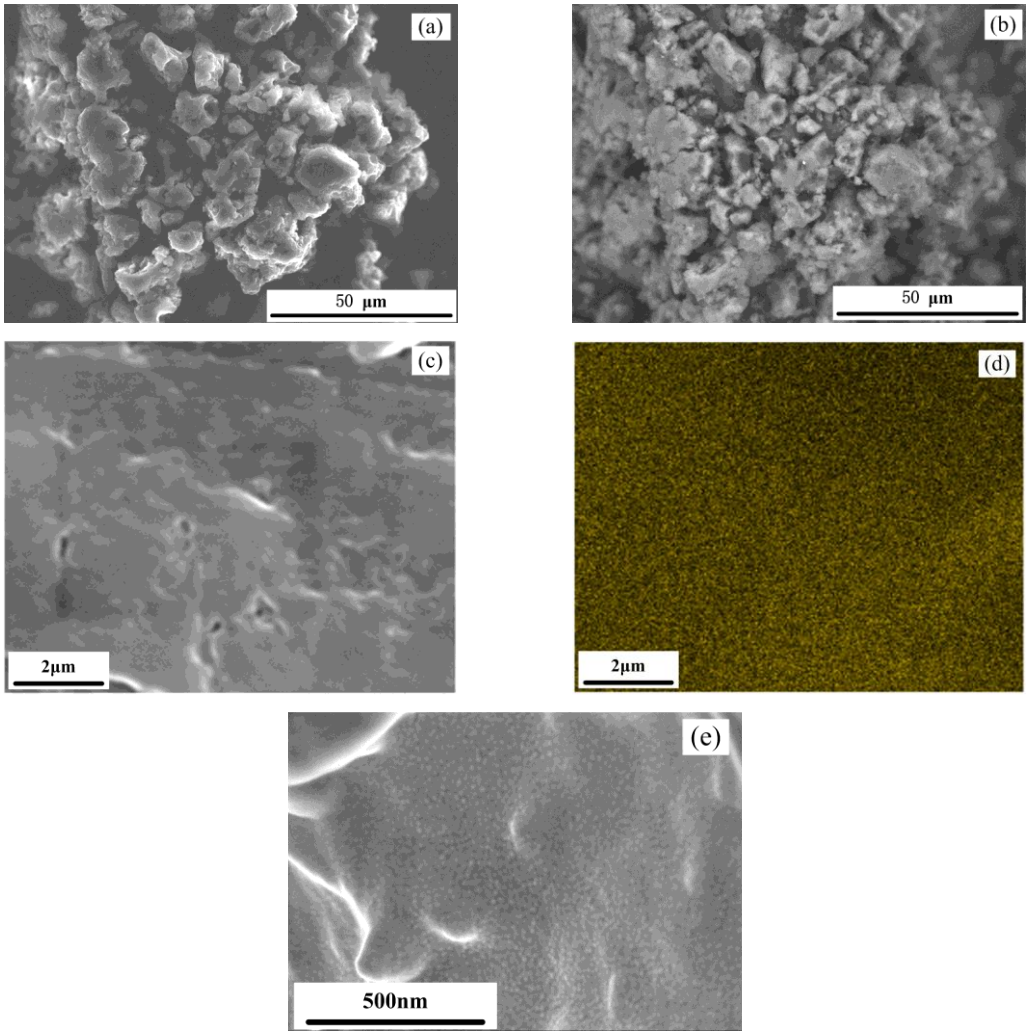

Fig. 2 SEM (a) and BSE (b) of PI/nano-SiO_2 powders (20 wt% nano-SiO_2); silicon mapping area (c), silicon mapping (d) and fracture surface (e) of PI/nano-SiO_2 molding specimens (20 wt% nano-SiO_2).

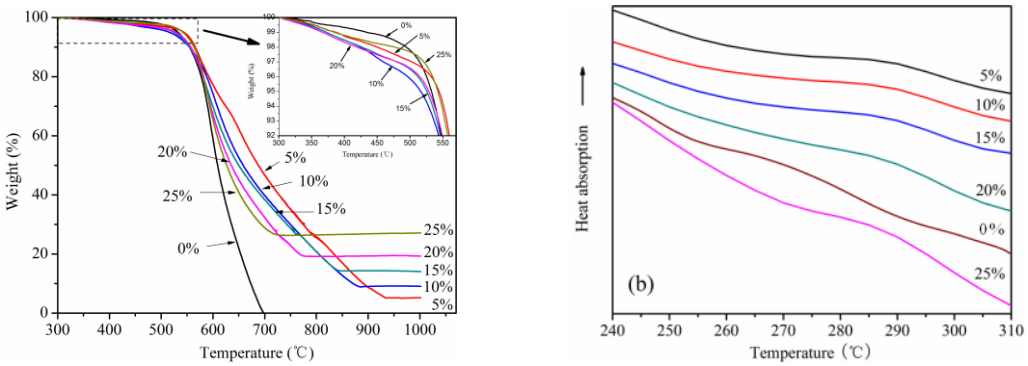

Fig. 3 (a) TG curves under air atmosphere, (b) DSC curves under argon atmosphere of pure PI and PI/nano-SiO_2 composites.

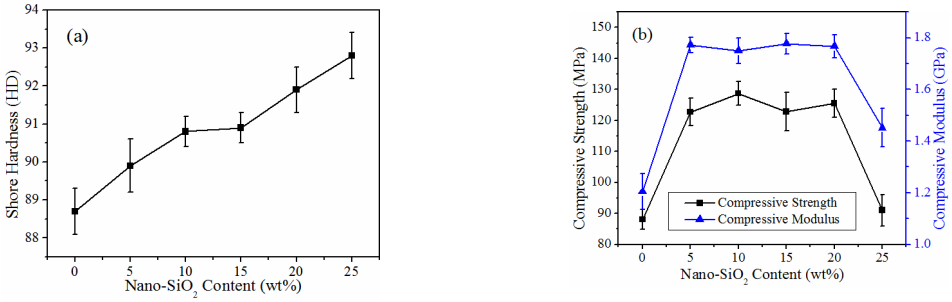

Fig. 4 Mechanical properties of PI/nano-SiO_2 composites with different nano-SiO_2 contents: (a) Shore hardness and (b) compressive strength and compressive modulus.

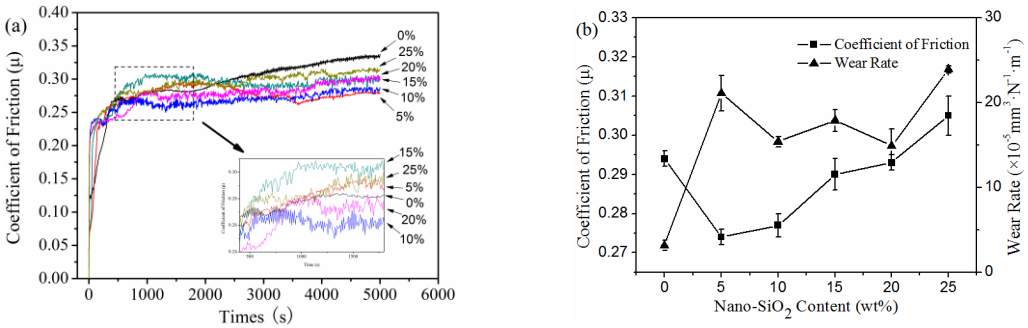

Fig. 5 (a) COF curves, (b) COF and wear rate of PI/nano-SiO_2 at the load of 10 N and sliding velocity of 0.08 m/s.

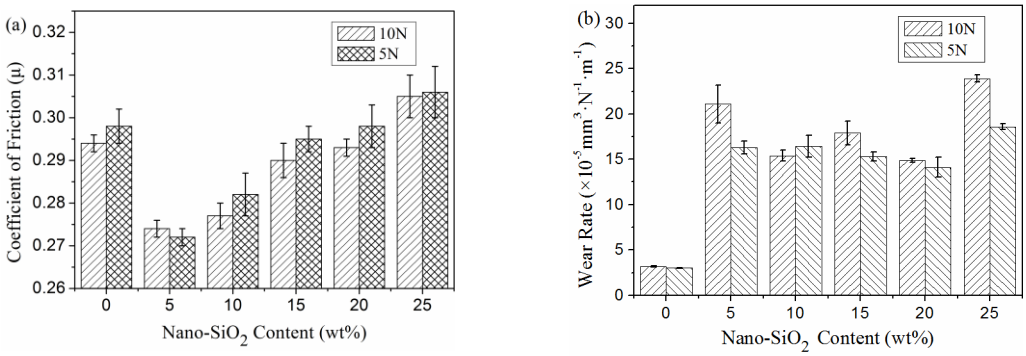

Fig. 6 Effects of loads on the COF and wear rate of PI/nano-SiO_2 composites as a function of Nano-SiO_2 content at a sliding velocity of 0.08 m/s.

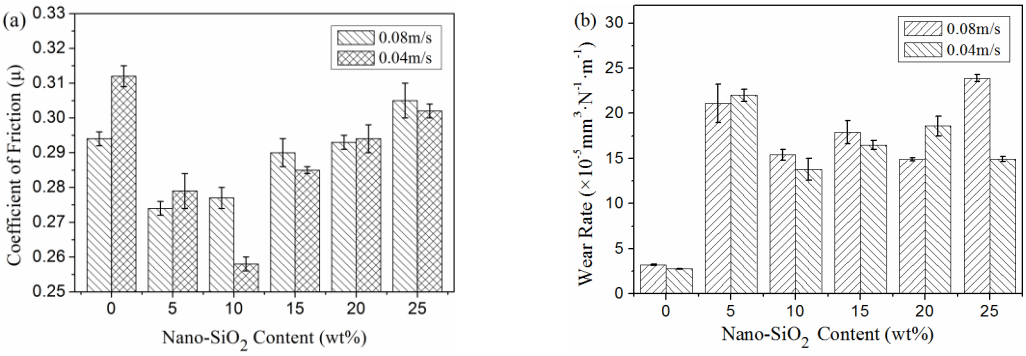

Fig. 7 Effects of sliding velocity on the COF and wear rate of PI/nano-SiO_2 composites under the load of 10 N.

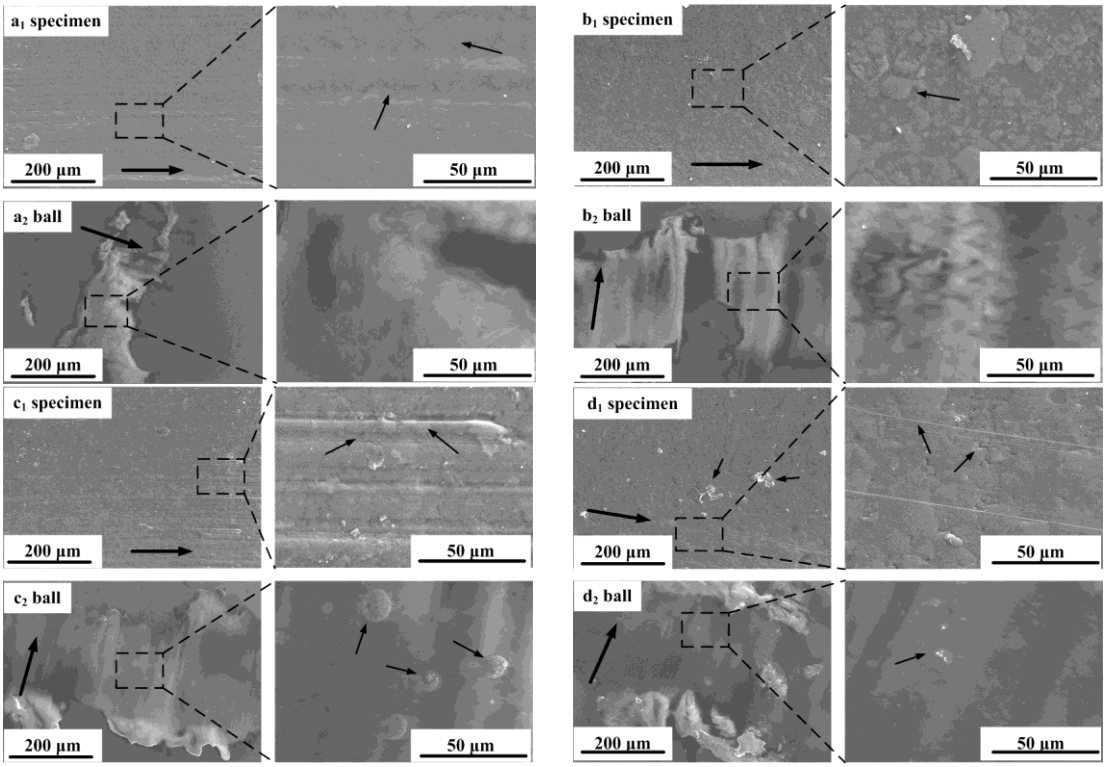

Fig. 8 SEM morphologies of worn surfaces of PI/nano-SiO_2 composite specimens and transfer films on a counterpart ball under the load of 10 N and sliding velocity of 0.08 m/s. (a) 5% nano-SiO_2, (b) 10% nano-SiO_2, (c) 15% nano-SiO_2, (d) 20% nano-SiO_2. The thick arrows indicate the sliding direction.

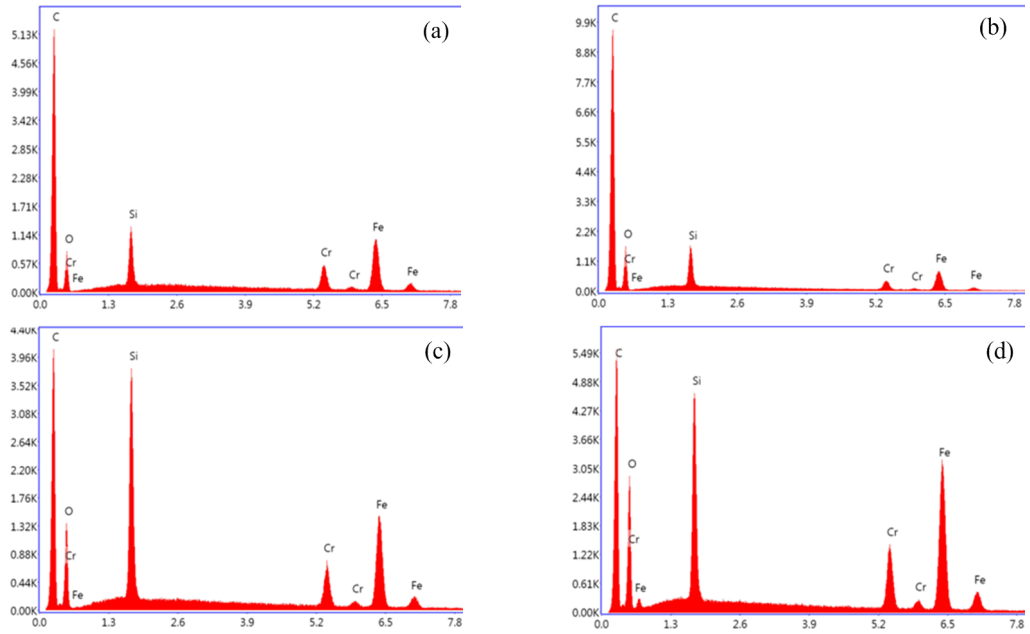

Fig. 9 EDS spectra of PI/nano-SiO_2 composites and counterpart transfer films with the load of 10 N and sliding velocity of 0.08 m/s at different nano-SiO_2 contents: (a) 5 wt%, (b) 10 wt%, (c) 15 wt% and (d) 20 wt%.